INVESTIGATIVE RADIOLOGY
Volume 37, Number 10, 571–576
©2002, Lippincott Williams & Wilkins, Inc.

Measurement of the Vascularity and Vascular Leakage of Gliomas by Double-Echo Dynamic Magnetic Resonance Imaging

A Preliminary Study

HIDEMASA UEMATSU, MD, PHD,* MASAYUKI MAEDA, MD, PHD,§ NORIHIRO SADATO, MD, PHD,¶ YOSHIYUKI ISHIMORI, RT,* TSUYOSHI MATSUDA, RT,‖ YOSHIO KOSHIMOTO, MD, PHD,* HIROHIKO KIMURA, MD, PHD,* HIROKI YAMADA, MD, PHD,* YASUTAKA KAWAMURA, MD, PHD,* HIROAKI TAKEUCHI, MD, PHD,† YOSHIHARU YONEKURA, MD, PHD,‡ AND HARUMI ITOH, MD, PHD*

Uematsu H, Maeda M, Sadato N, et al. Measurement of the vascularity and vascular leakage of gliomas by double-echo dynamic magnetic resonance imaging: A preliminary study. Invest Radiol 2002;37:571–576.

RATIONALE AND OBJECTIVE. **To evaluate the vascularity and vascular leakage of well-enhanced gliomas by double-echo dynamic magnetic resonance (MR) imaging.**

MATERIALS AND METHODS. **Eight patients with glioblastoma multiforme (GBM) and two patients with juvenile pilocytic astrocytoma (JPA) were studied. Double-echo dynamic MR imaging was utilized to separate the T2* shortening effect and the T1 shortening effect. The former was represented by the vascularity index, and the latter was represented by the leakage index. These indexes were compared with histopathologic data.**

RESULTS. **The mean vascularity index of the GBM was higher than that of the JPA (mean ± SD, 3.48 ± 1.57 [GBM] versus 0.51 ± 0.29 [JPA]), and the mean leakage index of the JPA was higher than that of the GBM (1.35 ± 0.87 [JPA] versus 0.27 ± 0.15 [GBM]). Abundant vascularity was noted in the tight interstitial space in the pathologic specimen of GBM. Conversely, sparse vasculature was observed in the wide interstitial space in the pathologic specimen of JPA.**

CONCLUSION. **This method may enable better characterization of grade in well-enhanced glioma by providing the information on the vascularity and leakage indexes.**

KEY WORDS. **Gliomas; vascular leakage; blood-brain barrier; vascularity; double-echo; contrast media; MR imaging.**

THE WORLD Health Organization (WHO) classification of tumors of the nervous system is an attempt to develop a standardized classification scheme with as few interpretative controversies as possible.[1] Tumor grading is based on several pieces of information, such as the presence or absence of cellular and nuclear pleomorphism, nuclear mitosis, necrosis, endothelial proliferation of the capillaries, and invasion. This WHO grading system can provide useful information regarding the treatment and patient prognosis. Thus, a good prognosis for a grade I tumor, such as a juvenile pilocytic astrocytoma (JPA), can be expected only by the removal of the tumor. However, a grade IV tumor, such as a glioblastoma multiforme (GBM), is considered to have an extremely poor prognosis.

Although examining the vascularity of gliomas by means of indicator dilution theory[2] is useful for characterizing the grade of glioma,[3–6] it needs to be taken into account that tumor vessels have another characteristic that is different from normally functioning blood vessels of the brain. This is caused by the absence of normal blood-brain barrier (BBB) function. To utilize the susceptibility effect of gado-

From the *Department of Radiology, the †Department of Neurosurgery, and the ‡Biomedical Imaging Research Center, Fukui Medical University, Fukui, Japan.

§From the Department of Radiology, Mie University School of Medicine, Mie, Japan.

¶From the Department of Cerebral Research, National Institute for Physiological Sciences, Okazaki, Japan.

‖From GE-Yokogawa Medical Systems, Tokyo, Japan.

Supported in part by a research grant (JSPS-RFTF97L00203) from the Japan Society for the Promotion of Science.

Reprint requests to: Hidemasa Uematsu, MD, PhD, Department of Radiology, University of Pennsylvania Medical Center, 3600 Market Street, Suite 370, Philadelphia, PA 19104-2649; E-mail: uematsu@oasis.rad.upenn.edu

Received February 9, 2002, and accepted for publication, after revision, June 18, 2002.

pentetate dimeglumine (Gd-DTPA) for the assessment of the vascularity of a brain tumor, the measured signal change must be linearly correlated with the local concentration of Gd-DTPA. However, after an intravenous bolus injection, there is prompt distribution of the Gd-DTPA through the vascular and extracellular spaces of the brain tumor. Thus, Gd-DTPA causes a T1 shortening and a T2* shortening effect once it has leaked into the interstitial space. The rate of diffusion is complex but depends in part on regional perfusion, actual permeability of the proliferating new vessels, and the size of the extracellular space within the tumor.[7] Hence, the signal intensity of the tumor derives not only from the vascularity but also from the permeability of tumor vessels and the size of interstitial space. To measure the exact concentration-time curve of Gd-DTPA, a T1-bias-free estimate of the concentration-time curve was obtained using the double-echo technique.[8,9]

To evaluate both vascularity and vascular leakage simultaneously, double-echo dynamic magnetic resonance (MR) imaging was applied. The vascularity was evaluated by the T2* shortening effect because of the intravascular fraction of Gd-DTPA, and the vascular leakage was evaluated by the T1 shortening effect using the extravascular fraction.[8,9] In this study, our aim was to evaluate the vascularity and vascular leakage (permeability of the tumor vessels and the size of the extracellular space within the tumor) and to compare them with histopathologic data.

Materials and Methods

Theory

After bolus injection, Gd-DTPA causes the T2* rate change ($\Delta R2^*$) in permeable tissue, which is contaminated by the T1 shortening effect because of a leakage of the contrast agent;[3–6,10,11] $\Delta R2^*_{T1U}(t)$ is calculated as follows:

$$\Delta R2^*_{T1U}(t) = -\ln(S/S_0)/TE \quad (1)$$

where $\Delta R2^*_{T1U}$ is the T1 uncorrected $\Delta R2^*$ from the single echo data, S represents the signal intensity at time t, S_0 represents the signal intensity before the arrival of the contrast agent, and TE represents the echo time. The T1 shortening effect can be corrected by the double-echo technique;[8,9] $\Delta R2^*_{T1C}(t)$ is calculated as follows:

$$\Delta R2^*_{T1C}(t) = [\ln(S_1/S_2)/(TE_2\text{-}TE_1)] - R2^*_{pre} \quad (2)$$

where $\Delta R2^*_{T1C}$ is the T1 corrected $\Delta R2^*$ by double-echo technique; S_1 and S_2 represent the signals of the first echo time (TE_1) and the second echo time (TE_2), respectively, and $R2^*_{pre}$ is the T2* rate before the arrival of the contrast agent. The difference between $\Delta R2^*_{T1C}(t)$ and $\Delta R2^*_{T1U}(t)$ is linearly (r^2=0.97) related to the concentration of the leaked contrast agent and can be used as an index for contrast leakage[8]:

$$\text{The leakage value} = \Delta R2^*_{T1C}(t) - \Delta R2^*_{T1U}(t)(t > t_0) \quad (3)$$

Note that the leakage value reflects the total amount of the leaked contrast agent.

The concentration-time curve ($\Delta R2^*_{T1C}$) was fitted to a γ-variate function to correct for recirculation. The vascularity value (relative blood volume) represents the area under this fitted concentration-time curve ($\Delta R2^*_{T1Cf}$) and is calculated using the following equation[2–6,8–12]:

$$\text{the vascularity value} = \int_0^\infty \Delta R2^*_{T1Cf}(t)\,dt \quad (4)$$

The vascularity value of the tumor can be normalized by the vascularity value of the reference tissue (white matter) to generate the vascularity index (VI). The leakage value can be normalized by the maximum height of the curve of $\Delta R2^*_{T1Cf}$ ($\Delta R2^*_{T1Cf}$ max) to derive the leakage index (LI):

$$\text{the leakage index} = \frac{\Delta R2^*_{T1C}(t) - \Delta R2^*_{T1U}(t)}{\Delta R2^*_{T1Cf}\text{max}} \quad (5)$$

As $\Delta R2^*_{T1Cf}$ max is known to be proportional to blood flow,[13] the LI reflects the contrast extraction fraction.

Subjects

Human studies were performed under the guidelines of our hospital committee on clinical investigations. Inclusion criterion for the patients of this study was the approval of the physician who referred them to this prospective MR study. Patients who had any of the following conditions were excluded: pacemaker, metal implants, risk for adverse reaction to intravenous injection of Gd-DTPA, the possibility of pregnancy, or mental illness. Written informed consent was obtained from all patients. Eight consecutive patients (six men and two women; aged 42–83 years; mean age: 61.3 years; median: 62 years) with GBM and two patients (one man and one woman; age 18 years for both patients) with JPA were investigated. Three of these GBM subjects had been included in another research protocol.[9] The maximum diameters of the GBM ranged from 0.86 to 6.0 cm (mean: 3.85 cm; median: 4.11 cm). The maximum diameters of the JPA were 0.8 and 4.64 cm, respectively. One patient with GBM underwent a stereotactic biopsy before MR examination. Four patients with GBM had been previously treated with surgical resection followed by irradiation and chemotherapy; however, prominent tumor regrowth was confirmed by follow-up CT and MR examinations. The radiologist (H.U.) who performed the data analysis was aware of the histologic results regarding these five GBM cases. In all patients, the presence of gliomas was histologically verified by surgical resection after MR studies.

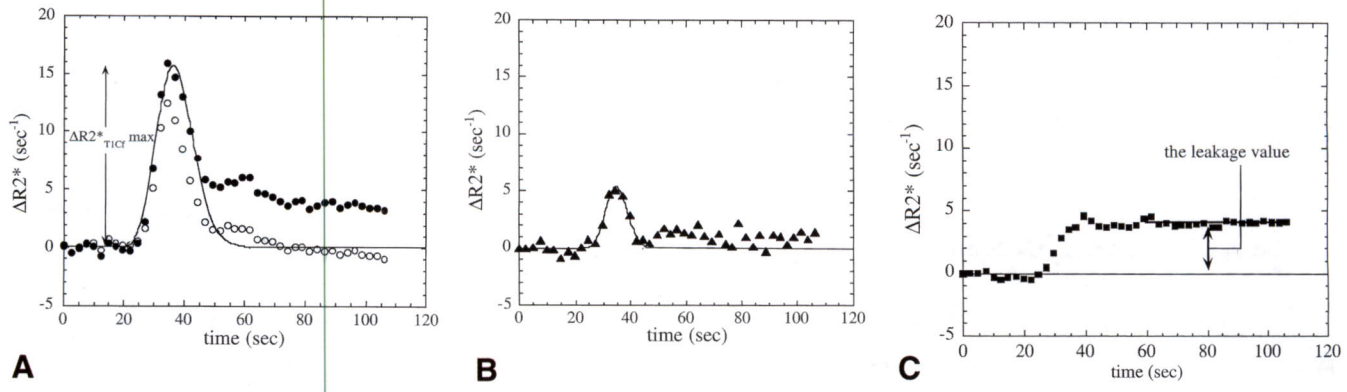

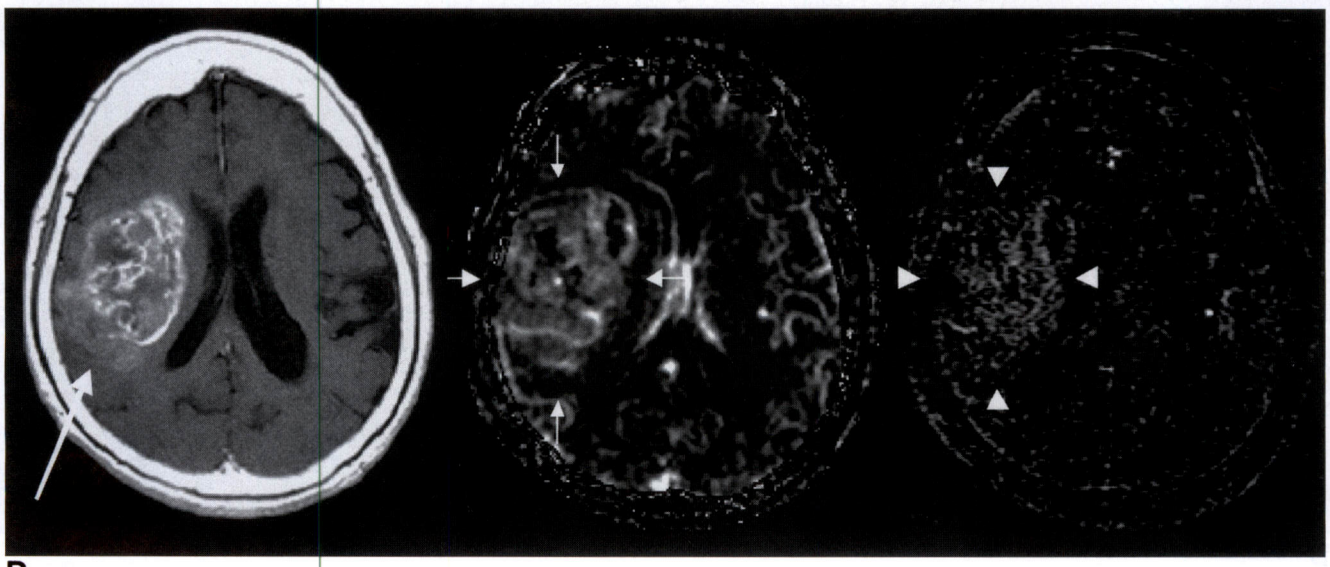

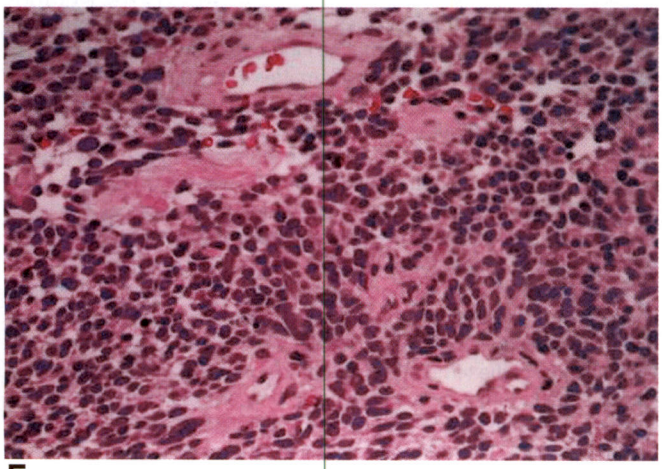

Figure 1. An example of glioblastoma multiforme (GBM). (A) Time course of the ΔR2* values of an 83-year-old male patient with GBM. The $\Delta R2^*_{T1C}$ values of the GBM are plotted by closed circles, its γ-fitted curve ($\Delta R2^*_{T1Cf}$) is represented by a solid line, and $\Delta R2^*_{T1U}$ is represented by open circles. (B) Time course of the ΔR2* values of the normal white matter of the same patient. The $\Delta R2^*_{T1C}$ values of the normal white matter are plotted by closed triangles, and its γ-fitted curve ($\Delta R2^*_{T1Cf}$) is represented by a solid line. (C) Time course of the leakage values of the GBM of the same patient. The leakage values are plotted by closed squares. The GBM is characterized by a low leakage value relative to the high $\Delta R2^*_{T1Cf}$ curve, resulting in a high VI and a relatively low LI. (D) Contrast-enhanced T1-weighted spin echo image (left), the vascularity value map (middle), and the leakage value map (right) of the same patient with GBM. T1-weighted spin echo image and parametric images are at slightly different angles. GBM shows inhomogeneous enhancement in the right front-parietal lobe (large white arrow). Note the high vascularity value (small white arrows) and relatively low leakage value (white arrowheads) of the tumor. (E) Histopathologic specimen of GBM of the same patient: high nuclear/cytoplasm tumor cells proliferating in a tight interstitial space with abundant vascularity and frequent mitosis (hematoxylin and eosin staining; ×200). This GBM is classified as Category 1.

Magnetic Resonance Imaging Techniques

Axial T1-weighted spin echo images (repetition time [TR]/echo time [TE]/number of excitations [NEX]: 333/10 ms/3) and T2-weighted fast spin echo images (TR/TE/NEX: 3500/88 ms/2) were obtained (rectangular field of view: 22 cm × 16 cm, matrix size: 256 × 224, slice thickness: 5 mm) using a 1.5 T MR system (Horizon, General Electric Medical Systems, Milwaukee, WI) before the dynamic study.

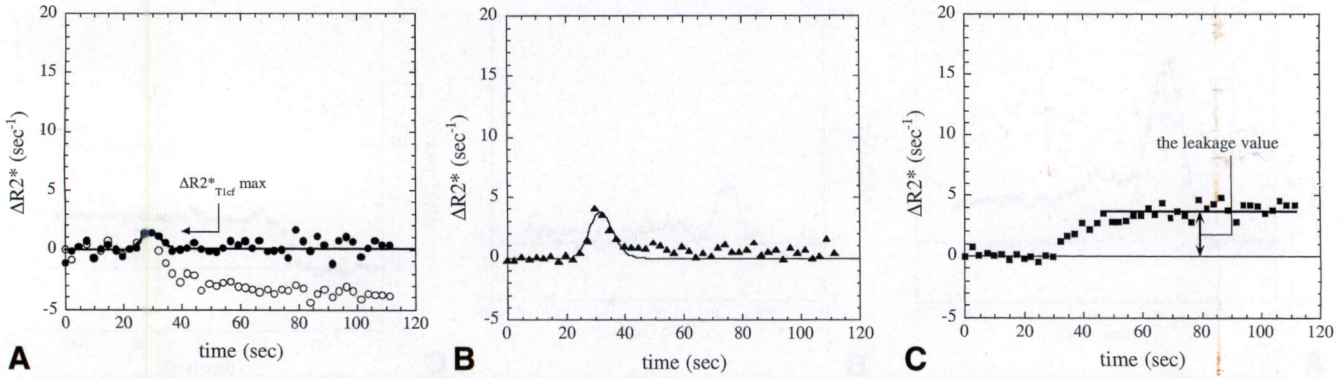

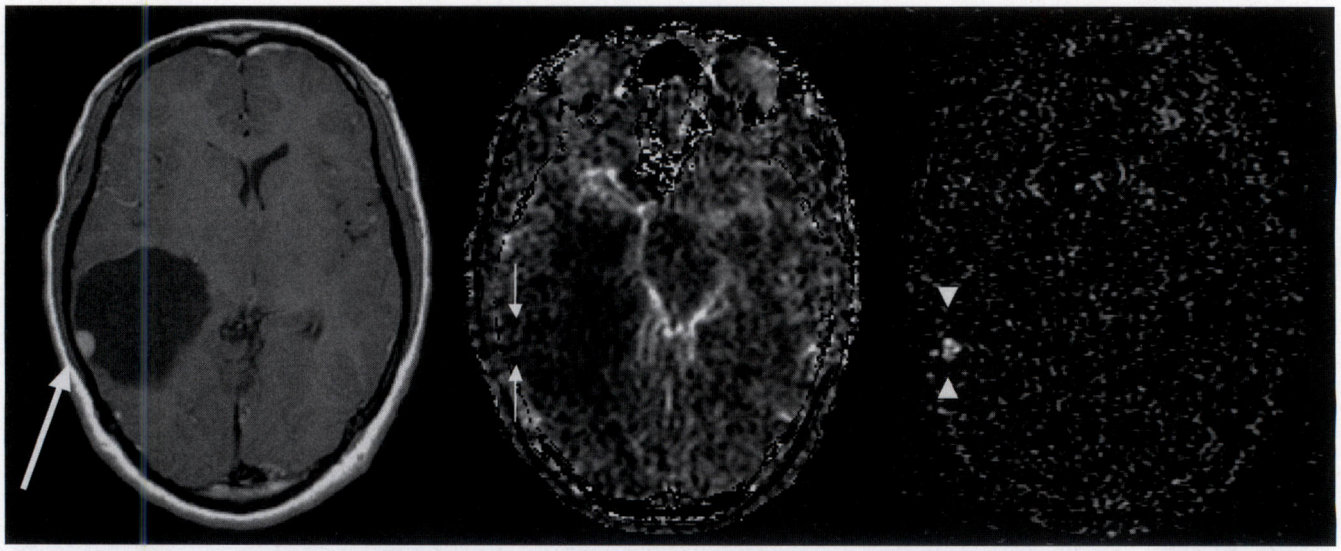

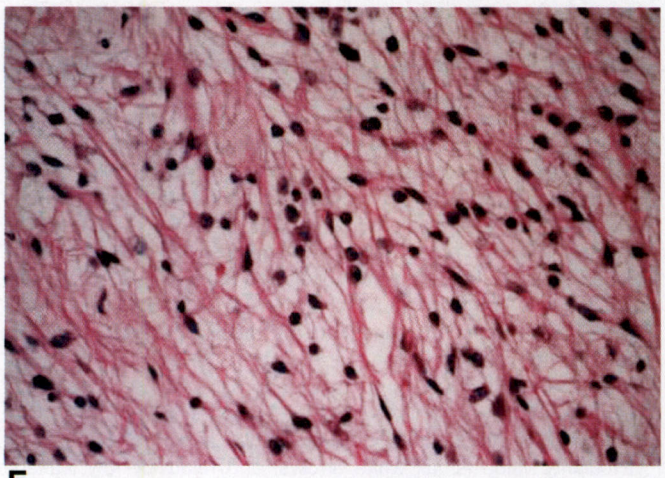

Figure 2. An example of juvenile pilocytic astrocytoma (JPA). (A) Time course of the ΔR2* values of an 18-year-old female patient with a JPA with the same format as Figure 1A. (B) Time course of the ΔR2* values of the normal white matter with the same format as Figure 1B. (C) Time course of the leakage values of the JPA with the same format as Figure 1C. The JPA is characterized by a low $\Delta R2^*_{T1Cf}$ curve relative to the leakage values, resulting in a high LI and low VI. (D) The contrast-enhanced T1-weighted spin echo image (left), the vascularity value map (middle), and the leakage value map (right) of the JPA in the right temporal lobe. T1-weighted spin echo image and parametric images are at slightly different angles. The JPA shows intense homogeneous enhancement in the solid portion of the tumors on the left image (white arrow). Note the low vascularity value (small white arrows) and high leakage value (white arrowheads) of the tumor. (E) Histopathologic specimens of JPA of the same patient: tumor cells with bipolar long processes proliferating in the wide interstitial space of sparse vasculature (hematoxylin and eosin staining; ×200). This JPA was classified as Category 4.

For single slice dynamic study, we used two echoes with TEs of 7 and 23 ms of a spoiled gradient recalled acquisition (SPGR) sequence ($TR/TE_1/TE_2$/flip angle: 33.3/7/23 ms/10°; NEX: 0.75; matrix size: 256 × 128; slice thickness: 7 mm; rectangular field of view: 24 cm × 16 cm). The slice that showed the largest solid portion was selected by the radiologist (H.U.) from the information obtained from these spin-echo MR images. The apparent hemorrhagic portion was not selected. After five images were acquired, 0.15 mmol/kg body weight Gd-DTPA (Magnevist, Nihon Schering, Osaka, Japan) was rapidly injected intravenously at a rate of 4 mL/second with an MR-compatible power injector

(MRS-50, Nemoto, Tokyo, Japan) followed by a 20-mL saline flush. After the bolus administration of Gd-DTPA, a dynamic series of 50 sets of double-echo images was obtained at 2.47-second intervals. For this sequence, the total acquisition time was approximately 2 minutes. After the dynamic studies, we also obtained contrast-enhanced T1-weighted spin echo images.

Data Analysis

MR images were transferred to a Sun workstation (Ultra1 creator 3D, Sun Microsystems, Mountain View, CA) for postprocessing. The vascularity value maps were generated for each subject using in-house software to choose the location with the greatest vascularity. On a pixel-by-pixel basis, the signal intensity was converted to changes in $\Delta R2^*_{T1C}$. We used a simple numerical integration of the time-$\Delta R2^*_{T1C}$ curve instead of gamma fitting because gamma fitting on a pixel-by-pixel basis was difficult because of the relatively low signal-to-noise ratio of the dynamic images.

For quantitative analysis, we did not place the regions of interest (ROIs) on the parametric maps. ROIs were placed on the SPGR images in the contra-lateral normal white matter and in the solid portion of the tumors, corresponding to the greatest vascularity value in the parametric map. The ROIs were placed by one radiologist (H.U.). Time series of signal intensities were converted to changes in $\Delta R2^*_{T1C}$ and $\Delta R2^*_{T1U}$. Gamma fitting of $\Delta R2^*_{T1C}$ was performed to generate $\Delta R2^*_{T1Cf}$. To obtain the leakage value, ($\Delta R2^*_{T1C} - \Delta R2^*_{T1U}$) values immediately after the first pass of time-$\Delta R2^*_{T1Cf}$ curve were averaged. The vascularity value was obtained by Eq. [4], and the VI of the tumor was calculated with the vascularity value of the tumor normalized by that of the contra-lateral white matter. The LI was then obtained by Eq. [5] These data were then compared with histopathologic data.

Pathologic Analysis

Tumor specimens in each patient were examined by a neuro-pathologist with hematoxylin and eosin staining. Categories for vascularity and cellularity were as follows: a high density of tumor cells proliferating with abundant vascularity in a tight interstitial space (Category 1); a high density of tumor cells proliferating with sparse vascularity in a tight interstitial space (Category 2); a low density of tumor cells proliferating in the wide interstitial space of abundant vasculature (Category 3); and a low density of tumor cells proliferating in the wide interstitial space of sparse vasculature (Category 4).

Results

In this study, all cases of JPA showed intense homogeneous enhancement in the solid portion of the tumors, and all cases of GBM showed inhomogeneous enhancement on contrast-enhanced T1-weighted spin echo MR images. In terms of vascularity and cellularity, all pathologic specimens of GBM were classified as Category 1. Pathologic analysis determined that the JPA specimens were classified as Category 4.

As shown in Figure 1A, B, C, a typical GBM was characterized by a low leakage value relative to the high $\Delta R2^*_{T1Cf}$ curve, resulting in a high VI and a relatively low LI (Fig. 1D). The histopathologic specimen of this patient is shown in Figure 1E. A high density of tumor cells proliferating with abundant vascularity in a tight interstitial space was noted in this specimen (Category 1).

As shown in Figure 2A, B, C, a typical JPA was characterized by a relatively high leakage value relative to the low $\Delta R2^*_{T1Cf}$ curve, and the vascularity value was much smaller than that of normal white matter. As shown in Figure 2D, this resulted in a low VI and high LI. The histopathologic specimen of this patient is shown in Figure 2E. A low density of tumor cells proliferating in a wide interstitial space of sparse vasculature was noted (Category 4). The mean VI of the GBM was higher than that of the JPA (mean ± SD, 3.48 ± 1.57 [GBM] versus 0.51 ± 0.29 [JPA]), and the mean LI of the JPA was higher than that of the GBM (1.35 ± 0.87 [JPA] versus 0.27 ± 0.15 [GBM]).

Discussion

In this study, GBM had a higher VI, which was consistent with pathologic examination; vascularity was markedly noted, and tumor cells were proliferating in a tight interstitial space as shown in Figure 1E. In previous reports,[4,5] the maximum VI of gliomas significantly correlated with both histologic and angiographic vascularities. In general, a malignant glioma has a higher vascularity.[3–6] This higher vascularity was confirmed in this study. However, the JPA, a subtype of low-grade astrocytoma, had a small VI. This low VI is supported by the pathologic analysis: a low density of tumor cells proliferating in a wide interstitial space of sparse vasculature, as shown in Figure 2E. From the histologic aspect, the vascular density of a JPA is similar to that of normal cerebellar white matter and is less vascular than an anaplastic astrocytoma.[14] The histologic specimen of JPA supported our MR data.

In this study, all cases of JPA showed intense homogeneous enhancement in the solid portion of the tumors, and all cases of GBM showed inhomogeneous enhancement on contrast-enhanced T1-weighted spin echo MR images. The widening of gap junctions of endothelial cells and endothelial fenestrations on electron microscopy cause a breakdown of the BBB in gliomas. However, no significant differences in these vascular structures were found between GBM and JPA in previous reports using electron microscopy.[15,16] From these observations using electron microscopy,[15,16] we speculate that the degree of vascular permeability is similar in GBM and JPA. In this study, GBM showed a high density of tumor cells proliferating in tight interstitial space on pathologic examination

whereas the JPA showed a low density of tumor cells proliferating in wide interstitial space. The diffusion of Gd-DTPA depends on the actual permeability of the proliferating new vessels and the size of the extracellular space within the tumor;[7] therefore, the difference in interstitial space might explain why, after the first transit, the contrast agent remained in the interstitial spaces in greater quantity in the JPA, causing a larger LI in the case of JPA.

This study included two types of gliomas (GBM and JPA). Because JPA is known to be completely different from GBM in pathologic structure, we examined these two types of tumors. Our study is observational and preliminary with a small sample size. Therefore, statistical analysis should not be applied to the current data. However, our intention was not to use our technique (VI and LI) as a diagnostic tool for the separation of the two types of gliomas. In general, it is easy to differentiate GBM from JPA by conventional MR imaging. Our purpose was to investigate vascular density and vascular leakage by utilizing the present MR method and to demonstrate a potential use of this technique.

Our study was limited. First and foremost, proper correlation between radiologic and pathologic data was not possible. The comparison between the MR images and the autopsy specimen might offer an answer to this issue; however, proper correlation between our technique (VI and LI) and pathologic data is impossible in the clinical setting. Second, our number of patients was limited, and the patients were confined to grades 1 and 4 of gliomas. Clinical concern will be whether those indexes can differentiate between gliomas of grades 2, 3, and 4. Further investigation into various types of gliomas using larger sample sizes will be necessary to clarify the potential of Vl and Ll for tumor tissue characterization.

Conclusion

In conclusion, although differentiating JPA and GBM produces little confusion using routine MR imaging in most cases, our preliminary data suggest that the LI and the VI can characterize gliomas with contrast enhancement.

Acknowledgments

The authors thank Hiroto Hatabu, MD, PhD, Hirotsugu Kado, MD, PhD, Hajime Sakuma, MD, PhD, and Kan Takeda, MD, PhD for their useful discussion; Hiroyuki Sashie, RT, Tomokazu Ishida, RT, Miho Takeuchi, RT, and Genji Asanuma, RT, for their assistance with MR data collection, and Lorene M. Yoxtheimer, BS, for her assistance with manuscript preparation.

References

1. Kleihues P, Cavenee WE, eds. World Health Organization classification of tumours: Pathology and genetics of tumours of the nervous system. Lyon, France: International Agency for Research on Cancer (IARC) Press; 2000.
2. Axel L. Cerebral blood flow determination by rapid-sequence computed tomography: theoretical analysis. Radiology 1980;137:679–686.
3. Maeda M, Itoh S, Kimura H, et al. Tumor vascularity in the brain: evaluation with dynamic susceptibility- contrast MR imaging. Radiology 1993;189:233–238.
4. Aronen HJ, Gazit IE, Louis DN, et al. Cerebral blood volume maps of gliomas: comparison with tumor grade and histologic findings. Radiology 1994;191:41–51.
5. Sugahara T, Korogi Y, Kochi M, et al. Correlation of MR imaging-determined cerebral blood volume maps with histologic and angiographic determination of vascularity of gliomas. AJR 1998;171: 1479–1486.
6. Knopp EA, Cha S, Johnson G, et al. Glial neoplasms: dynamic contrast-enhanced T2*-weighted MR imaging. Radiology 1999; 211:791–798.
7. Bullock PR, Mansfield P, Gowland P, et al. Dynamic imaging of contrast enhancement in brain tumors. Magn Reson Med 1991;19: 293–298.
8. Uematsu H, Maeda M, Sadato N, et al. Vascular permeability: quantitative measurement with double-echo dynamic MR imaging–theory and clinical application. Radiology 2000;214:912–917.
9. Uematsu H, Maeda M, Sadato N, et al. Blood volume of gliomas determined by double-echo dynamic perfusion- weighted MR imaging: a preliminary study. AJNR Am J Neuroradiol 2001;22: 1915–1919.
10. Maeda M, Itoh S, Kimura H, et al. Vascularity of meningiomas and neuromas: assessment with dynamic susceptibility-contrast MR imaging. AJR 1994;163:181–186.
11. Bruening R, Wu RH, Yousry TA, et al. Regional relative blood volume MR maps of meningiomas before and after partial embolization. J Comput Assist Tomogr 1998;22:104–110.
12. Martel AL, Allder SJ, Delay GS, et al. Perfusion MRI of infarcted and noninfarcted brain tissue in stroke: a comparison of conventional hemodynamic imaging and factor analysis of dynamic studies. Invest Radiol 2001;36:378–385.
13. Muramoto S, Uematsu H, Sadato N, et al. $H_2{}^{15}$ 0 PET validation of tumor blood flow determined by double echo dynamic perfusion-weighted MR imaging. J Comput Assist Tomogr 2002 (in press).
14. Sato K, Rorke LB. Vascular bundles and wicker works in childhood brain tumors. Pediatr Neurosci 1989;15:105–110.
15. Nir I, Levanon D, Iosilevsky G. Permeability of blood vessels in experimental gliomas: Uptake of 99mTc- glucoheptonate and alteration in blood-brain barrier as determined by cytochemistry and electron microscopy. Neurosurgery 1989;25:523–531.
16. Long DM. Capillary ultrastructure and the blood-brain barrier in human malignant brain tumors. J Neurosurg 1970;32:127–144.